

LAA-Net: A Physical-prior-knowledge Based Network for Robust Nighttime Depth Estimation

Kebin Peng¹, Haotang Li², Zhenyu Qi², Huashan Chen³, Zi Wang⁴, Wei Zhang⁴, Sen He²

East Carolina University¹
University of Arizona²
Chinese Academy of Sciences³
Augusta University⁴

Abstract

Existing self-supervised monocular depth estimation (MDE) models attempt to improve nighttime performance by using GANs to transfer nighttime images into their daytime versions. However, this can introduce inconsistencies due to the complexities of real-world daytime lighting variations, which may finally lead to inaccurate estimation results. To address this issue, we leverage physical-prior-knowledge about light wavelength and light attenuation during nighttime. Specifically, our model, Light-Attenuation-Aware Network (LAA-Net), incorporates physical insights from Rayleigh scattering theory for robust nighttime depth estimation: LAA-Net is trained based on red channel values because red light preserves more information under nighttime scenarios due to its longer wavelength. Additionally, based on Beer-Lambert law, we introduce Red Channel Attenuation (RCA) loss to guide LAA-Net’s training. Experiments on the RobotCar-Night, nuScenes-Night, RobotCar-Day, and KITTI datasets demonstrate that our model outperforms SOTA models.

1. Introduction

Monocular depth estimation (MDE) estimates the distances from a single image, which is an essential task for autonomous driving and robotics navigation. For MDE tasks, amongst learning-based approaches, self-supervised MDE models have been widely adopted by state-of-the-art techniques due to their effectiveness and cost efficiency [33]. However, MDE under nighttime scenarios are understudied because of low visibility and varying lighting conditions. Specifically, unlike daytime self-supervised MDE models [39], nighttime self-supervised MDE models pose a significant challenge: *the lack of a reliable self-supervised signal under nighttime scenarios* [33, 38].

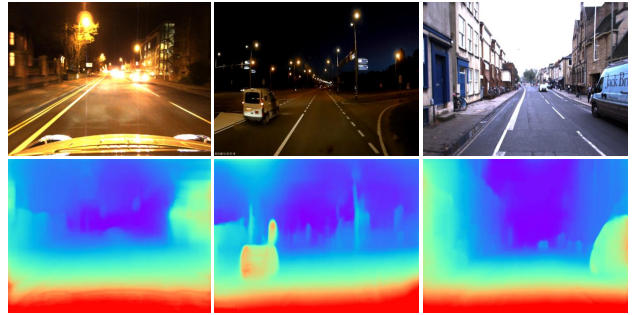


Figure 1. MDE results of LAA-Net on nighttime (left and middle) and daytime (right) images from Oxford RobotCar dataset [19].

To work around the challenge, SOTA methods [4, 17, 31, 33] have adopted GANs to synthetically convert nighttime inputs into their daytime counterparts, and then, the depth maps are estimated based on the converted images. However, during the conversion, the complex real-world lighting conditions may result in discrepant simulations, eventually leading to inaccurate depth estimation results.

To tackle the challenge, we propose a novel and efficient self-supervised model for nighttime MDE by incorporating two physical-prior-knowledge: Rayleigh scattering theory and Beer-Lambert law.

Rayleigh Scattering Theory depicts the relationship between wavelength and the amount of scattered light (Equation 1). Specifically, *red light, due to its longer wavelength, is less likely to get scattered at night than blue and green light. Thus, red light preserves more information under nighttime scenarios.* Based on this observation, we propose Light-Attenuation-Aware Network (LAA-Net), a physical-prior-knowledge based network for robust nighttime depth estimation. Figure 2 illustrates the architecture of LAA-Net. We first use the red channel values of each pixel as inputs during Light Attenuation module training (Figure 2 - a). In this way, LAA-Net effectively learns the relationship

between the red channel values and depth values. Then, we concatenate the Light Attenuation module with our depth estimation network (Figure 2 - b2). By adopting Rayleigh scattering theory, LAA-Net eliminates the need to convert nighttime images into daytime versions, which ensures the reliability, accuracy, and robustness of our MDE model.

Beer-Lambert Law describes that light attenuation is proportional to distance (Equation 2). Based on Beer-Lambert law and Rayleigh scattering theory, we introduce Red Channel Attenuation (RCA) loss (Equation 5). This loss function is used to guide the training process of LAA-Net. Thus, LAA-Net becomes capable of learning the connections between depth values and red channel attenuation.

Figure 1 shows the MDE results using LAA-Net have clear edges and accurate depth values under both nighttime and daytime scenarios. It is mainly because the adopted **Rayleigh scattering theory and Beer-Lambert law are physical-prior-knowledge, which indicates that they hold true despite the time of the day**. Thus, incorporating physical-prior-knowledge ensures our model’s accuracy, generality, and robustness.

In summary, the key contributions of this paper include:

- 1) We find that Rayleigh scattering theory and Beer-Lambert law can be used to enhance the accuracy and robustness of nighttime monocular depth estimation.
- 2) We observe that nighttime MDE relies primarily on the textural patterns of an object rather than its color. Using red channel images as input leads to enhanced MDE performance, especially in low-light conditions.
- 3) Based on Rayleigh scattering theory and Beer-Lambert law, we implement a physical-prior-knowledge based nighttime depth estimation model: LAA-Net and a reliable self-supervised signal under nighttime scenarios: RCA loss.
- 4) A thorough evaluation of the proposed model demonstrates that LAA-Net improves MDE under both nighttime and daytime scenarios.

2. Related Work

Daytime Depth Estimation: Self-supervised depth estimation has received a lot of attention in recent years. Zhou et al. [39] and Godard et al. [7] are two of the pioneer works that used self-supervised MDE approaches to train the depth network in conjunction with a separate pose network. Later, Godard et al. [8] proposed a minimum reprojection loss and a full-resolution multi-scale sampling method to train the depth estimation network. To solve the occlusion issue, Godard et al. [9] improved their prior work [8] by introducing randomized layer normalization and a new regularizer. Later, Guizilini et al. [10] use symmetrical packing/unpacking blocks and 3D convolutions in outdoor scenes. Klingner et al. [14] use supervised semantic segmentation and self-supervised depth estimation to deal with

moving objects.

Nighttime Depth Estimation: The difficulty of obtaining ground truth images leads to many self-supervised approaches being developed for nighttime depth estimation. For example, Vankadari et al. [31] view the nighttime depth estimation as a domain adaptation problem, and they adapted a network trained on daytime images to function in nighttime conditions. Then, Sharma et al. [26] developed a translation network to create nighttime stereo images from daytime versions, and a stereo network was trained based on the created images for nighttime depth estimation. Later, Lu et al. [18] combined thermal and RGB data to enhance the accuracy of nighttime depth estimation. Recently, Gasperini et al. [4] used a translation model to convert nighttime images into daytime conditions; then, the converted images are used for nighttime MDE tasks.

3. Proposed Model

In this paper, we develop LAA-Net, a novel and robust self-supervised network, to estimate the depth under nighttime scenarios. Section 3.1 illustrates the network architecture of LAA-Net (Figure 2), which contains DispNet for depth estimation and SfMLearner for pose estimation. Section 3.2 discusses our observation that using red channel images for nighttime MDE yields better results. Section 3.3 details the design of the Rayleigh-scattering-theory-based Light Attenuation module (Figure 2 - a). To guide the training process of this module, in Section 3.4, we introduce RCA loss (Figure 2 - d), which is based on Beer-Lambert law and Rayleigh scattering theory. In Section 3.5, photometric reconstruction loss function [39] with pose estimation network (Figure 2 - c) is adopted to assist RCA loss to serve as robust self-supervised signals for nighttime MDE.

3.1. Network Architecture

Depth Estimation CNN: We choose the DispNet architecture proposed in [20, 39]. It is primarily built on an encoder-decoder architecture with skipped connections and multi-scale side prediction. Meanwhile, all CNN layers are followed by ReLU activation except for the prediction layers. Regarding the prediction layers, like Zhou et al. [39], we use $\frac{1}{\alpha \cdot \text{sigmoid}(x) + \beta}$ with $\alpha = 10$ and $\beta = 0.0125$ to constrain the predicted depth to be always positive within a reasonable range (e.g., 80 meters). For comparison, we also set β to different values to constrain the range to 40, 50, and 60 meters, respectively; the results are shown in supplementary material. In addition, we use a DenseASPP module [37] with dilation rates $r \in \{3, 6, 12, 18, 24\}$ between the encoder and decoder to further improve the accuracy of the baseline. The output from the last three convolution layers in the Light Attenuation module is concatenated along channel direction with three convolution layers in DispNet Decoder (Figure 2 - a).

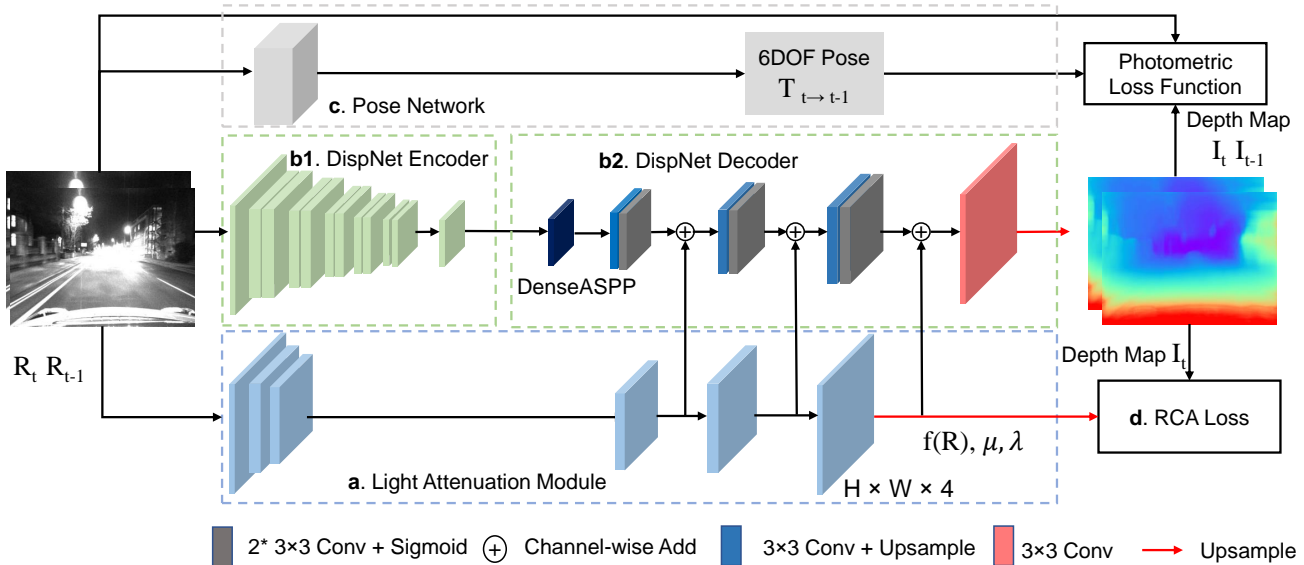


Figure 2. **LAA-Net Architecture** contains three parts: (a) Light Attenuation module (blue box) provides physical-prior-knowledge to depth estimation module (green boxes) and serves as the input of RCA loss. $f(R)$ means the feature from the last layer of Light Attenuation module. (b) Self-supervised Depth Estimation network which contains a DispNet Encoder(b1) and Decoder(b2). The DispNet Encoder outputs an image feature map. The feature map then goes through a decoder, which we use to generate the depth map. (c) Pose Estimation Network (gray box) outputs 6D pose information that could be used with the depth map as a supervised signal for MDE.

Pose Estimation CNN: The pose estimation network learns a pose transformation between two consecutive frames, which serves as a part of our self-supervised signals for depth estimation. We follow the same network in SfMLearner [39], in which we concatenate two consecutive frames along the channel direction. The concatenated result is fed into the Pose Estimation CNN. The outputs are the relative poses between each of the source views and the target view. Specifically, the network consists of 2 convolutions followed by a 1×1 convolution with 6×1 output channels. One channel corresponds to 3 Euler angles and a 3-D translation for each source view. All convolution layers are followed by ReLU except for the last layer, where no nonlinear activation is applied. Since we use photometric reconstruction loss function \mathcal{L}_p from SfMLearner [39] during the training processes, which implies that the rigid assumptions in SfMLearner [39] also apply to our model.

3.2. Red Channel Image for Nighttime MDE

As reviewed in Section 2, due to the lack of a robust self-supervised signal under nighttime scenarios, SOTA methods rely on GAN-based models to convert nighttime images to their daytime versions for nighttime depth estimation. However, the intricate nature of real-world lighting conditions makes it difficult to accurately generate daytime images, leading to disparities from their real-world equivalents. For example, light intensity is one of the most complex elements in real-world lighting conditions; light intensity varies due to factors like weather conditions (sunny,

cloudy, etc.) and time of day (morning, noon, etc.). These varying factors affect the appearance of object textures under different lighting conditions. Without adequately covering all the factors, it is easy to create discrepant simulations and, eventually, inaccurate depth estimation results.

To address the limitations, we propose to build a robust nighttime MDE model by enabling depth estimation directly from nighttime images without daytime conversions. Our initial step is to delve into the input data. **First**, according to Torralba et al. [29], texture variations often correlate with changes in depth. Specifically, texture changes across an image (e.g., getting smaller or denser), enabling models to understand the relative distance of objects. Geirhos et al. [6] further show that CNNs predominantly learn patterns from image textures. **Second**, based on Rayleigh scattering theory, green and blue light, due to their shorter wavelengths, are more prone to be scattered at night, which means that green and blue light are less likely to preserve complete texture information under nighttime scenarios.

Thus, We conduct experiments to see the relationships between image channels and the accuracy of nighttime MDE results. Particularly, we use DispNet and pose estimation network mentioned in Section 3.1 as the baseline model, and then, RGB images from RobotCar-Night dataset [19] are replaced by their single-channel images and two-channel images for comparison. Table 1 shows that single-channel image settings outperform their two-channel counterparts, surpassing RGB image settings. Notably, the red channel setting (Baseline+R) yields the best results.

Table 1. **Using Different Channel Images from RobotCar-Night Dataset [19]:** R means Red Channel, so do B (Blue Channel) and G (Green Channel), RGB. The best results are in **bold**.

Methods	Abs Rel	Sq Rel	RMSE	RMSE log
	lower is better			
Baseline+RGB	0.675	8.215	7.105	0.473
Baseline+B+R	0.673	8.211	7.105	0.473
Baseline+G+R	0.675	8.212	7.103	0.471
Baseline+B+G	0.671	8.210	7.104	0.469
Baseline+B	0.668	8.209	7.098	0.465
Baseline+G	0.667	8.209	7.098	0.463
Baseline+R	0.665	8.206	7.097	0.461

This is because *red channel has the best texture retention due to Rayleigh scattering theory; furthermore, this setting eliminates the detrimental influence of potentially being "noised" by incomplete texture information from green and blue channels*. Therefore, **LAA-Net is designed to use red channel images for better accuracy and robustness**.

3.3. Light Attenuation Module

To take full advantage of red channel images, we propose Light Attenuation module (Figure 2 - a), which aims to enable DispNet and pose estimation network to *explicitly and comprehensively* learn the relationships between red channel values and depth values. As discussed in Section 3.2, the design is based on Rayleigh scattering theory, which states that the amount of light scattering is inversely proportional to the wavelength. As shown in Equation 1, I_s is the intensity of scattered light, and λ is the wavelength. Red light has the largest λ value, leading to the smallest I_s . Thus, the inputs of Light Attenuation module are red channel images, which only contain red channel values.

$$I_s \propto \frac{1}{\lambda^4} \quad (1)$$

To implement Light Attenuation module, we employ the U-Net architecture [25] to extract image features and establish the correlation between red channel values and depth values (Figure 2 - a). To enhance the robustness of our depth estimation process, we concatenate the outputs from the U-Net decoder with the output of the DispNet Decoder along the channel direction (Figure 2 - b2). Note that the difference in output dimensions between U-Net and DispNet decoders requires a down-sampling layer for compatibility.

The output of Light Attenuation module is the predicted depth map from red channel image. It also serves as part of the inputs of RCA loss (See Section 3.4). Simultaneously, the predicted depth map from the DispNet decoder serves as the other part of RCA loss input. To match the dimensions of the predicted depth map, the last layer of Light Attenuation module’s output requires an up-sampling layer. One noteworthy difference between Light Attenuation module and the original U-Net is that, while they both output the same dimension for depth estimation, Light Attenuation module, in addition, outputs additional two channels for estimating μ and λ for RCA loss in Equation 5.

3.4. Red Channel Attenuation Loss (RCA loss)

To guide the training processes of Light Attenuation module, we introduce RCA loss (Figure 2 - d). RCA loss is based on Beer-Lambert law (Equation 2) and Rayleigh scattering theory (Equation 1).

$$I = I_0 e^{-\mu d_R} \quad (2)$$

Beer-Lambert Law describes that light attenuation is proportional to distance. Specifically, in our model, we consider Equation 2 for each pixel, where I_0 denotes the intensity of the luminous point. I denotes the light intensity after attenuation. μ is a constant and d is depth value. $e^{-\mu d_R}$ is the attenuation item. Also, we discuss the different items in Section 9 in Supplementary Material.

Equation 2 suggests the possibility of deriving the depth value, denoted as d_R from the information contained in I and I_0 . This insight motivates us to employ it as a loss function during the training of Light Attenuation module. To facilitate this, we rephrase Equation 2 to Equation 3 as:

$$d_R = -\frac{1}{\mu} \ln I + \frac{\ln I_0}{\mu} \quad (3)$$

We then use gradient Spherical Gaussian (SG) [15, 32, 35] to model I_0 in Equation 4, where $\lambda \in \mathbb{R}$ is a learnable parameter to capture the underlying distribution of I_0 , enabling Light Attenuation module to dynamically adapt to the intensity changes of the luminous point. In our experiments, we empirically set $g = 1.3938$ for the best accuracy.

$$I_0 = e^{g\lambda - 1} \quad (4)$$

Additionally, as discussed in Section 3.2 and Section 3.3, the phenomenon of Rayleigh scattering theory drives our decision to focus on the attenuation of red channel in our architecture. Thus, we replace the RGB image I with red channel image R , and $f(R)$ represents the feature from the last layer of Light Attenuation module. Taking gradient SG and $f(R)$ into account, we can now reformulate Equation 3 to Equation 5 as follow:

$$d_R = -\frac{1}{\mu} \ln f(R) + \frac{1}{\mu} (g\lambda - 1) \quad (5)$$

In light of the preceding discussion, we apply Equation 5 to train Light Attenuation module. Specifically, when we know d_R , we use \mathcal{L}_2 to denote L2 loss and compute \mathcal{L}_2 between d_R and d_{ES} . d_{ES} is the estimated depth map from DispNet decoder. *Because the attenuation has a functional relation $\ln f(R)$ with depth value d_R , it can be used to supervise the training of Light Attenuation module*, which is the mathematical foundation of our design choice.

3.5. Total Training Loss Function

RCA loss serves as a self-supervised signal to guide the training processes of Light Attenuation module. Besides RCA loss, we also train our model with another supervisory signal: photometric reconstruction loss function \mathcal{L}_p from SfMLearner [39]. It requires four inputs as Figure 2 shows: Image I_t, I_{t-1} , Transformation $T_{t \rightarrow t-1}$, predicted depth map D_t , and camera intrinsics matrix K . The total loss function is $\mathcal{L} = \mathcal{L}_p + \mathcal{L}_2$.

4. Experiments

Implementation Details: Our model is built using PyTorch [23]. We train our model with a batch size of 4, Adam optimizer [13] is used with $\beta_1 = 0.9$ and $\beta_2 = 0.999$, we set the learning rate to 0.0002. Meanwhile, we follow Zhou et al. [39], which we multiply the predicted depth maps by a scalar \hat{s} to match the median with the groundtruth, i.e., $\hat{s} = \text{median}(D_{gt}) / \text{median}(D_{pred})$.

Datasets: We evaluate LAA-Net on two nighttime datasets (RobotCar-Night [19] and nuScenes-Night [1]) and two daytime datasets (RobotCar-Day [19] and KITTI [5]) to demonstrate that *LAA-Net is accurate and robust under both nighttime and daytime scenarios*. Our model is trained on those four datasets, respectively. For baselines, we use any provided training weights from the original authors. If not provided, then we use the training weights of KITTI [5]; afterwards, these weights are fine-tuned on all datasets for a fair comparison. More details about the training and testing on the datasets could be referred to Section 8 in Supplementary Material.

4.1. Results

We evaluate our proposed model both quantitatively and qualitatively. For quantitative analysis, we perform the comparison against SOTA methods on all four datasets mentioned above. We use seven metrics, same as those used in [2, 8] - Abs Rel, Sq Rel, RMSE, RMSE_{log} , $\delta < 1.25$, $\delta < 1.25^2$, and $\delta < 1.25^3$. For qualitative analysis, we compare estimated depth maps from LAA-Net and SOTA models using images from RobotCar-Night, and KITTI.

Quantitative Results: Tables 2, 3, and 4 show the quantitative results on the Oxford RobotCar (both Night and Day), nuScenes-Night, and KITTI datasets, respectively. As Table 2 and 3 show, our model outperforms all SOTA models across all metrics, emphasizing its overall robustness and superior accuracy. In Table 4, our model performs better than all other SOTA models in all metrics except for CADepth-Net in RMSE_{log} , however, our model maintains the second-best and outperforms CADepth-Net in all other metrics. This could be attributed to the Light Attenuation module and RCA loss modeling the physical laws of Rayleigh scattering theory and Beer-Lambert law. These

physical laws, held both *daytime* and *nighttime*, are more effective than other previously adopted domain-specific features in improving MDE (ADDS [17], and ADFA [31]).

Among Tables 2, 3, and 4, md4All [4] is a strong baseline, which adopts GAN-based model and odometry information to achieve better performance. RNW [33] is another strong baseline, which performs better than other SOTA by using image enhancement module to enhance image visibility and contrast. CADepth-Net [36] is also a strong baseline, which has better performance due to the utilization of a channel-wise attention block. For other baselines, DIFFNet [22] proposed gradient information; EPCDepth [24] proposed data grafting from long-range correlation. FM [27] proposed Feature-metric loss, and PlaneDepth [34] proposed orthogonal-planes-based depth estimation. Overall, LAA-Net surpasses these baselines because *we considered light attenuation for red channel images, which is more robust and effective in improving depth estimation accuracy*.

Qualitative Results: Figure 3 shows the results on the RobotCar-Night dataset, qualitatively demonstrating that LAA-Net provides more accurate nighttime MDE results across varying nighttime lighting conditions. Specifically, the red boxes in Figure 3 - a highlight LAA-Net’s ability to accurately estimate depth in extremely low-light conditions. While our depth map clearly delineates the car, ADDS fails to capture the car’s boundary; ADAF and MonoDepth2 detect the car, but their outputs contain blurred car boundaries. This is because LAA-Net depends on the red channel, which preserves more complete texture information and minimizes noise from other channels under extreme low-lighting conditions. Moreover, in Figure 3 - c, LAA-Net effectively captures the car’s boundary while other SOTA models all fail to estimate the car’s back windshield area due to low-light and reflection, showcasing LAA-Net’s robustness under challenging nighttime lighting conditions.

Figure 4 illustrates the results on the KITTI dataset, indicating that LAA-Net, initially designed for nighttime MDE, outperforms SOTA models under daytime scenarios. For example, in Figure 4 - b, our model accurately detects the car, providing clear and sharp boundaries. In contrast, MonoDepth2 fails to detect the car entirely. While ADDS, EPCDepth, and DIFFNet are capable of locating the car, the boundaries they produce are noticeably blurred, making the two cars jammed together on the estimated depth maps. Similarly, in Figure 4 - d, the red box highlights that our model successfully detects the two small objects with precise outlines. Meanwhile, ADDS fails to detect the objects; the outputs from EPCDepth, MonoDepth2, and DIFFNet show unclear and blurred boundaries. *The good performance of LAA-Net under daytime scenarios can be attributed to the adopted physical laws because they hold both during nighttime and daytime*.

Ablation Study: Table 5 shows the impact of the Light

Table 2. **Quantitative Results - RobotCar-Night and RobotCar-Day [19]:** We scale depth up to 80 meters. The best results are in **bold** for each metric. The results presented here are without post-processing. AD and DD mean different training strategies for md4All.

Methods	Abs Rel	Sq Rel	RMSE	RMSE log	$\delta < 1.25$	$\delta < 1.25^2$	$\delta < 1.25^3$
Test on RobotCar-Night							
	lower is better				higher is better		
SfMLearner [39]	0.675	8.215	7.105	0.473	0.655	0.803	0.961
MonoDepth2 [8]	0.399	7.451	6.641	0.442	0.744	0.892	0.928
DeFeat-Net [28]	0.392	4.895	6.342	0.423	0.625	0.829	0.899
ADFA [17]	0.233	3.783	10.089	0.319	0.668	0.844	0.924
ADDS [31]	0.231	2.674	8.800	0.286	0.620	0.892	0.956
EPCDepth [24]	0.165	0.912	4.531	0.192	0.897	0.852	0.921
RNW [33]	0.151	0.818	4.575	0.223	0.879	0.968	0.989
SGDepth [14]	0.129	0.981	4.455	0.207	0.831	0.944	0.977
md4All-AD [4]	0.124	0.788	3.612	0.178	0.858	0.902	0.971
md4All-DD [4]	0.122	0.784	3.604	0.175	0.849	0.913	0.958
LAA-Net	0.117	0.776	3.525	0.160	0.901	0.972	0.991
Test on RobotCar-Day							
	lower is better				higher is better		
MonoDepth2 [8]	0.120	0.718	3.245	0.315	0.864	0.871	0.935
md4All-AD [4]	0.112	0.742	3.308	0.165	0.882	0.927	0.980
md4All-DD [4]	0.113	0.648	3.206	0.163	0.871	0.910	0.968
LAA-Net	0.110	0.591	3.198	0.162	0.891	0.959	0.995

Table 3. **Quantitative Results - nuScenes-Night [1]:** We scale depth up to 80 meters. The best results are in **bold** for each metric. All results presented here are without post-processing. AD and DD mean different training strategies for md4All.

Methods	Abs Rel	Sq Rel	RMSE	RMSE log	$\delta < 1.25$	$\delta < 1.25^2$	$\delta < 1.25^3$
	lower is better				higher is better		
RNW [33]	0.290	4.169	11.289	1.569	0.557	0.621	0.743
MonoDepth2 [8]	0.147	1.755	6.941	1.813	0.827	0.851	0.899
md4All-AD [4]	0.141	1.691	6.915	0.475	0.830	0.895	0.912
md4All-DD [4]	0.128	1.502	6.607	0.468	0.845	0.901	0.933
LAA-Net	0.118	1.489	6.549	0.437	0.853	0.925	0.941

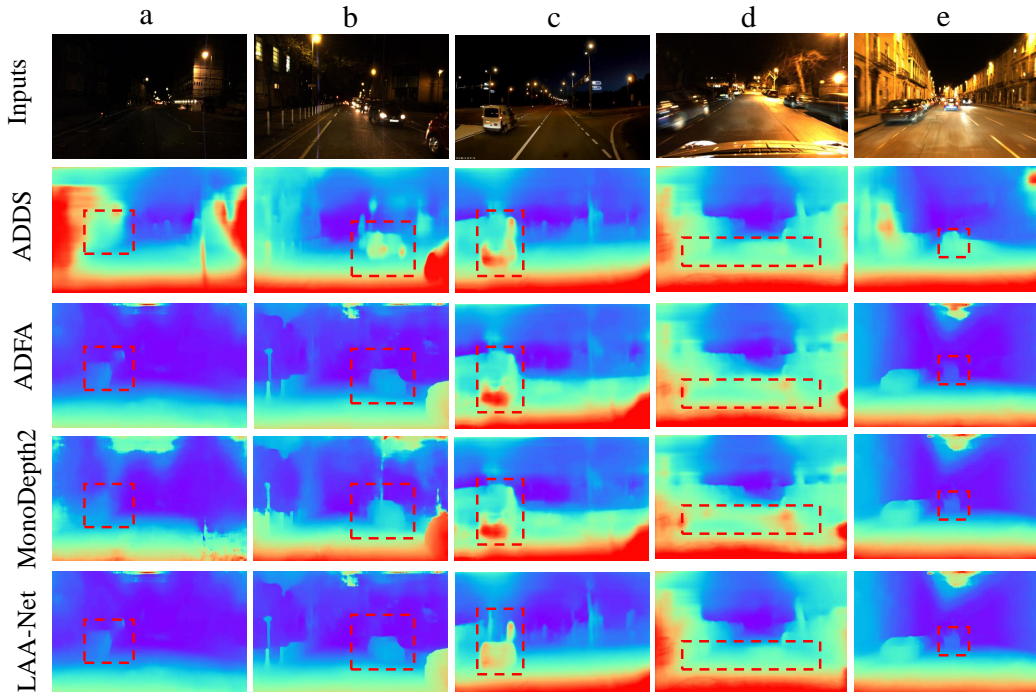


Figure 3. **Qualitative Results - RobotCar-Night:** Depth estimated on five different test images (row: Inputs) using our model (row: LAA-Net) and three SOTA (remaining rows) for comparison.

Attenuation module and RCA loss on our MDE model’s accuracy. Specifically, we conducted two ablation studies, one training on nighttime images from the RobotCar-Night dataset and the other training on daytime images from the

KITTI dataset. The results demonstrated the necessity of both Light Attenuation module and RCA loss in our model.

In Table 6, our model is trained on channel-specific images from the RobotCar-Night dataset and KITTI dataset.

Table 4. **Quantitative Results - KITTI [5]:** Comparison of our model on the KITTI test split by Eigen [2]. M means monocular image, and S means stereo image. The best results are in **bold** for each metric. All results presented here are without post-processing.

Methods	Data	$H \times W$	Abs Rel	Sq Rel	RMSE	RMSE log	$\delta < 1.25$	$\delta < 1.25^2$	$\delta < 1.25^3$
			lower is better				higher is better		
MonoDepth2 [8]	MS	320×1024	0.106	0.806	4.630	0.193	0.876	0.958	0.980
CADepth-Net [36]	MS	320×1024	0.096	0.694	4.264	0.173	0.908	0.968	0.984
PlaneDepth [34]	MS	384×1280	0.090	0.584	4.130	0.182	0.896	0.962	0.981
LAA-Net	MS	320×1024	0.088	0.579	4.037	0.180	0.912	0.971	0.988
DynaDepth [3]	S	192×640	0.109	0.787	4.705	0.195	0.869	0.958	0.981
MonoDepth2 [8]	S	320×1024	0.107	0.849	4.764	0.201	0.874	0.953	0.977
EPCDepth [24]	S	320×1024	0.091	0.646	4.207	0.176	0.901	0.966	0.983
DepthFormer [16]	S	320×1024	0.090	0.661	4.149	0.175	0.905	0.967	0.984
PlaneDepth [34]	S	384×1280	0.083	0.533	3.919	0.167	0.913	0.969	0.985
LAA-Net	S	320×1024	0.079	0.528	3.915	0.062	0.917	0.973	0.985
SfMLearner [39]	M	128×416	0.198	1.836	6.565	0.275	0.718	0.901	0.960
DeFeat-Net [28]	M	352×480	0.126	0.925	5.035	0.200	0.862	0.954	0.980
CADepth-Net [36]	M	192×640	0.105	0.769	4.535	0.181	0.892	0.964	0.983
FM [27]	M	192×640	0.104	0.729	4.481	0.179	0.893	0.965	0.984
GCP-MonoViT [21]	M	192×640	0.096	0.696	4.327	0.174	0.904	0.968	0.985
LAA-Net	M	192×640	0.096	0.613	4.013	0.170	0.906	0.969	0.987
MonoDepth2 [8]	M	320×1024	0.115	0.882	4.701	0.190	0.879	0.961	0.982
DynamicDepth[3]	M	192×640	0.103	1.000	5.867	0.157	0.897	0.964	0.984
CADepth-Net [36]	M	320×1024	0.102	0.734	4.407	0.178	0.898	0.966	0.984
DIFFNet [22]	M	320×1024	0.097	0.722	4.345	0.174	0.907	0.967	0.984
LAA-Net	M	320×1024	0.095	0.610	3.995	0.155	0.912	0.970	0.990

Table 5. **Ablation Study:** LAA-Net on all images from the RobotCar-Night dataset [19] (upper) and KITTI [5] (lower). We scale depth up to 80 meter. ResNet-50 means using ResNet-50 as the encoder to replace DispNet encoder. The baseline model is SfMLearner with DensASPP. LA means Light Attenuation module. RCA means RCA loss. The best results are in **bold**.

RobotCar-Night							
	Abs Rel	Sq Rel	RMSE	RMSE log	$\delta < 1.25$	$\delta < 1.25^2$	$\delta < 1.25^3$
	lower is better				higher is better		
Baseline	0.675	8.215	7.105	0.473	0.655	0.803	0.961
Baseline+LA	0.314	5.670	4.310	0.478	0.678	0.750	0.789
ResNet-50+LA	0.218	3.674	4.312	0.381	0.775	0.848	0.881
ResNet-50+LA+RCA	0.121	0.843	3.676	0.175	0.879	0.951	0.987
Baseline+LA+RCA	0.117	0.776	3.525	0.160	0.901	0.972	0.991
KITTI							
	Abs Rel	Sq Rel	RMSE	RMSE log	$\delta < 1.25$	$\delta < 1.25^2$	$\delta < 1.25^3$
	lower is better				higher is better		
Baseline	0.119	0.654	4.265	0.195	0.818	0.911	0.960
Baseline+LA	0.112	0.638	4.123	0.181	0.857	0.943	0.971
ResNet-50+LA	0.109	0.625	4.127	0.185	0.849	0.936	0.970
ResNet-50+LA+RCA	0.102	0.621	4.021	0.178	0.895	0.962	0.981
Baseline+LA+RCA	0.099	0.613	4.013	0.170	0.901	0.969	0.987

Those channels are: red channel(R), blue channel(B), green channel(G), and three-channels (RGB). As shown in Table 6, the LAA-Net+R only uses the red channel, which outperforms all other channel/channel-combinations, validating the foundations of our model design: 1) *using red channel images as input*; 2) *adopting physical-prior-knowledge to enhance the accuracy and robustness of MDE*.

Particularly, the findings in Table 6 and in Table 1 are consistent. We can observe that using single-channel image settings (R, G, or B) performs better than using two-channel image (R+G, R+B, or G+B). While using two-channel image settings outperforms using three-channel (RGB) images. This can be attributed to the fact that: *combining multiple channels could introduce noise, especially in low-light conditions* (e.g., Green and Blue channels could lose texture information due to Rayleigh scattering theory). That is, the additional channels (Green and Blue), instead of contribut-

ing significantly useful texture information, could "noise" the primary channel (Red) and confuse depth estimation models, leading to compromised MDE results.

Additionally, the red channel performs best among all single-channel settings, followed by the green channel; the blue channel performs the worst. The results yield with Rayleigh scattering theory (Equation 1) that $Scattering_{red} < Scattering_{green} < Scattering_{blue}$.

We also test LAA-Net with multiple views (3, and 5 views) as input. However, the results exhibit negligible improvements, aligning with the conclusions of Ummenhofer et al. [30] and Zhou et al. [39].

The supplementary material includes additional results and discussions, such as an ablation study on various light attenuation functions, analyses of different depth ranges, additional qualitative results, failure cases, etc.

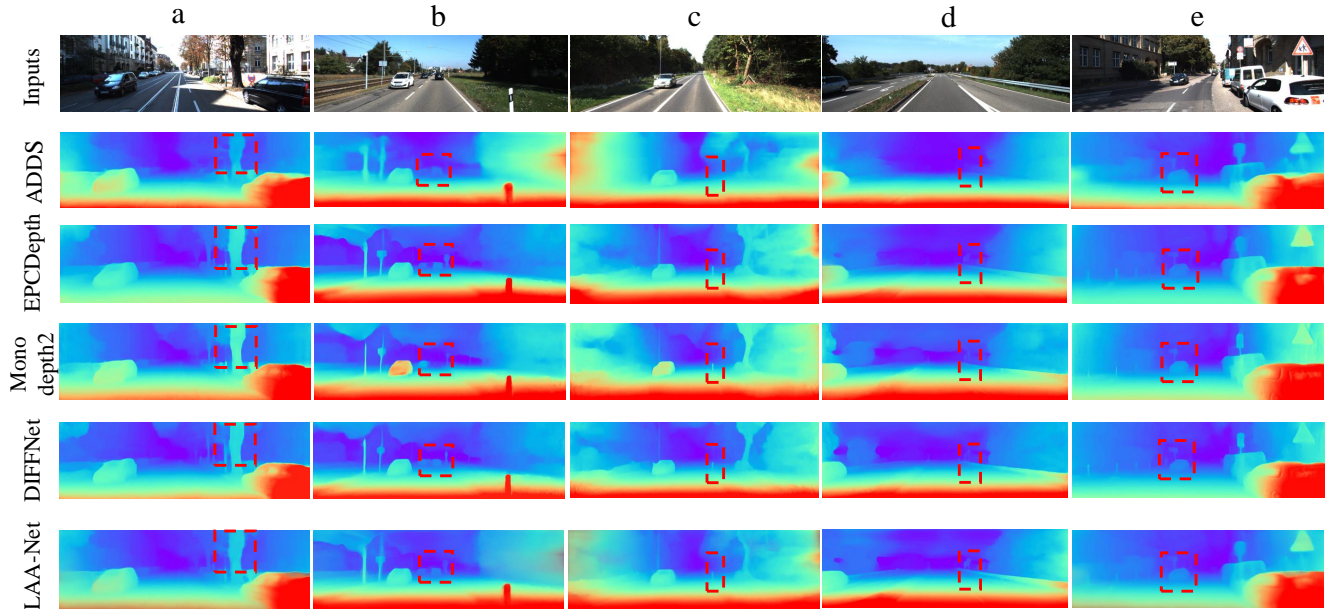


Figure 4. **Qualitative Results - KITTI**: Depth estimated on five different test images (row: Inputs) using our model (row: LAA-Net) and four SOTA (remaining rows) for comparison.

Table 6. **Ablation Study of Using Different Channel Images on RobotCar-Night Dataset [19] and KITTI Dataset [5]**: R means Red Channel, so do B (Blue Channel) and G (Green Channel), RGB. The best results are in **bold**.

RobotCar-Night				
Methods	Abs Rel	Sq Rel	RMSE	RMSE log
	lower is better			
LAA-Net+RGB	0.171	0.897	4.028	0.195
LAA-Net+B+R	0.155	0.852	3.921	0.182
LAA-Net+G+R	0.156	0.854	3.897	0.185
LAA-Net+B+G	0.159	0.857	3.842	0.188
LAA-Net+B	0.120	0.785	3.540	0.171
LAA-Net+G	0.119	0.780	3.531	0.168
LAA-Net+R	0.117	0.776	3.525	0.160
KITTI				
LAA-Net+RGB	0.157	0.975	4.857	0.212
LAA-Net+B+R	0.149	0.852	4.437	0.190
LAA-Net+G+R	0.147	0.801	4.339	0.185
LAA-Net+B+G	0.145	0.798	4.242	0.189
LAA-Net+B	0.110	0.651	4.240	0.181
LAA-Net+G	0.107	0.638	4.234	0.171
LAA-Net+R	0.095	0.610	3.995	0.155

5. Limitations and Future works

Although LAA-Net performs better than SOTA methods under both nighttime and daytime scenarios, we recognize certain limitations in LAA-Net and will focus on addressing them in our future research.

The first limitation is when it rains or snows during the

daytime. Compared with GAN-based approaches, such as md4All [4], LAA-Net exhibits constrained enhancements. This is because LAA-Net mainly focuses on addressing lighting conditions. Unlike nighttime scenarios, when it rains or snows during the daytime, the impact of daytime lighting conditions is relatively diminished for depth estimation. In our future work, new physical-law-based models will be explored to enhance depth estimation accuracy in extreme daytime weather conditions.

Another limitation is that we did not incorporate odometry information into LAA-Net. Odometry data, known for its robustness compared to image features, can be used to enhance pose estimation accuracy [4]. To overcome this limitation, our future work will integrate LAA-Net with multiple sensor fusion.

Finally, LAA-Net outperforms md4All [4] under both daytime and nighttime conditions. But consider the benefit of GAN-based MDE models: converting images to user-designated versions. In our future work, we will add GAN-based modules to LAA-Net to handle extreme nighttime weather conditions.

6. Conclusion

In this paper, we find that Rayleigh scattering theory and Beer-Lambert law can be used to improve nighttime monocular depth estimation, suggesting that incorporating more physical-prior-knowledge could potentially be beneficial in enhancing depth estimation accuracy. By incorporating Rayleigh scattering theory and Beer-Lambert law, we im-

plement LAA-Net, a novel red channel image-based self-supervised deep neural network for enhancing monocular depth estimation under both nighttime and daytime scenarios. To guide the training process, we introduce RCA loss, a reliable self-supervised signal under nighttime scenarios for LAA-Net. LAA-Net and RCA loss are highly robust because they are grounded in physical laws; furthermore, the proposed model is mathematically well-founded. According to the thorough evaluation, LAA-Net can significantly improve the depth estimation accuracy, robustness, and generality under both nighttime and daytime scenarios.

References

- [1] Holger Caesar, Varun Bankiti, Alex H Lang, Sourabh Vora, Venice Erin Liong, Qiang Xu, Anush Krishnan, Yu Pan, Giancarlo Baldan, and Oscar Beijbom. nuscenes: A multi-modal dataset for autonomous driving. In *Proceedings of the IEEE/CVF conference on computer vision and pattern recognition*, pages 11621–11631, 2020. 5, 6, 1
- [2] David Eigen, Christian Puhersch, and Rob Fergus. Depth map prediction from a single image using a multi-scale deep network. *Advances in neural information processing systems*, 27, 2014. 5, 7, 1
- [3] Ziyue Feng, Liang Yang, Longlong Jing, Haiyan Wang, YingLi Tian, and Bing Li. Disentangling object motion and occlusion for unsupervised multi-frame monocular depth. In *Computer Vision – ECCV 2022*, pages 228–244, Cham, 2022. Springer Nature Switzerland. 7
- [4] Stefano Gasperini, Nils Morbitzer, HyunJun Jung, Nassir Navab, and Federico Tombari. Robust monocular depth estimation under challenging conditions. In *Proceedings of the IEEE/CVF International Conference on Computer Vision*, pages 8177–8186, 2023. 1, 2, 5, 6, 8, 3, 4
- [5] Andreas Geiger, Philip Lenz, and Raquel Urtasun. Are we ready for autonomous driving? the kitti vision benchmark suite. In *2012 IEEE Conference on Computer Vision and Pattern Recognition*, pages 3354–3361. IEEE, 2012. 5, 7, 8, 1
- [6] Robert Geirhos, Patricia Rubisch, Claudio Michaelis, Matthias Bethge, Felix A. Wichmann, and Wieland Brendel. Imagenet-trained CNNs are biased towards texture; increasing shape bias improves accuracy and robustness. In *International Conference on Learning Representations*, 2019. 3
- [7] Clément Godard, Oisín Mac Aodha, and Gabriel J Brostow. Unsupervised monocular depth estimation with left-right consistency. In *Proceedings of the IEEE conference on computer vision and pattern recognition*, pages 270–279, 2017. 2
- [8] Clément Godard, Oisín Mac Aodha, Michael Firman, and Gabriel J Brostow. Digging into self-supervised monocular depth estimation. In *Proceedings of the IEEE/CVF International Conference on Computer Vision*, pages 3828–3838, 2019. 2, 5, 6, 7, 3
- [9] Ariel Gordon, Hanhan Li, Rico Jonschkowski, and Anelia Angelova. Depth from videos in the wild: Unsupervised monocular depth learning from unknown cameras. In *Proceedings of the IEEE/CVF International Conference on Computer Vision*, pages 8977–8986, 2019. 2
- [10] Vitor Guizilini, Rares Ambrus, Sudeep Pillai, Allan Raventos, and Adrien Gaidon. 3d packing for self-supervised monocular depth estimation. In *Proceedings of the IEEE/CVF conference on computer vision and pattern recognition*, pages 2485–2494, 2020. 2
- [11] Kaiming He, Xiangyu Zhang, Shaoqing Ren, and Jian Sun. Deep residual learning for image recognition. In *Proceedings of the IEEE conference on computer vision and pattern recognition*, pages 770–778, 2016. 1
- [12] <https://wiki.ogre3d.org/>. Point light attenuation, 2011. 1
- [13] Diederik P Kingma and Jimmy Ba. Adam: A method for stochastic optimization. *arXiv preprint arXiv:1412.6980*, 2014. 5
- [14] Marvin Klingner, Jan-Aike Termöhlen, Jonas Mikolajczyk, and Tim Fingscheidt. Self-supervised monocular depth estimation: Solving the dynamic object problem by semantic guidance. In *European Conference on Computer Vision*, pages 582–600. Springer, 2020. 2, 6
- [15] Zhengqin Li, Jia Shi, Sai Bi, Rui Zhu, Kalyan Sunkavalli, Miloš Hašan, Zexiang Xu, Ravi Ramamoorthi, and Manmohan Chandraker. Physically-based editing of indoor scene lighting from a single image. In *European Conference on Computer Vision*, pages 555–572. Springer, 2022. 4
- [16] Zhenyu Li, Zehui Chen, Xianming Liu, and Junjun Jiang. Depthformer: Exploiting long-range correlation and local information for accurate monocular depth estimation. *Machine Intelligence Research*, 20(6):837–854, 2023. 7
- [17] Lina Liu, Xibin Song, Mengmeng Wang, Yong Liu, and Liangjun Zhang. Self-supervised monocular depth estimation for all day images using domain separation. In *Proceedings of the IEEE/CVF International Conference on Computer Vision*, pages 12737–12746, 2021. 1, 5, 6
- [18] Yawen Lu and Guoyu Lu. An alternative of lidar in nighttime: Unsupervised depth estimation based on single thermal image. In *Proceedings of the IEEE/CVF Winter Conference on Applications of Computer Vision*, pages 3833–3843, 2021. 2
- [19] Will Maddern, Geoff Pascoe, Chris Linegar, and Paul Newman. 1 Year, 1000km: The Oxford RobotCar Dataset. *The International Journal of Robotics Research (IJRR)*, 36(1):3–15, 2017. 1, 3, 4, 5, 6, 7, 8
- [20] Nikolaus Mayer, Eddy Ilg, Philip Hausser, Philipp Fischer, Daniel Cremers, Alexey Dosovitskiy, and Thomas Brox. A large dataset to train convolutional networks for disparity, optical flow, and scene flow estimation. In *Proceedings of the IEEE conference on computer vision and pattern recognition*, pages 4040–4048, 2016. 2
- [21] Jaeho Moon, Juan Luis Gonzalez Bello, Byeongjun Kwon, and Munchurl Kim. From-ground-to-objects: Coarse-to-fine self-supervised monocular depth estimation of dynamic objects with ground contact prior. In *Proceedings of the IEEE/CVF Conference on Computer Vision and Pattern Recognition*, pages 10519–10529, 2024. 7
- [22] Juhung Park, Woojin Jung, Eun-Jung Choi, Se-Hong Oh, Jinhee Jang, Dongmyung Shin, Hongjun An, and Jongho Lee. Diffnet: Diffusion parameter mapping network generalized for input diffusion gradient schemes and b-value. *IEEE Transactions on Medical Imaging*, 41(2):491–499, 2021. 5, 7
- [23] Adam Paszke, Sam Gross, Francisco Massa, Adam Lerer, James Bradbury, Gregory Chanan, Trevor Killeen, Zeming Lin, Natalia Gimelshein, Luca Antiga, Alban Desmaison, Andreas Köpf, Edward Yang, Zach DeVito, Martin Raison, Alykhan Tejani, Sasank Chilamkurthy, Benoit Steiner, Lu Fang, Junjie Bai, and Soumith Chintala. *PyTorch: an imperative style, high-performance deep learning library*. Curran Associates Inc., Red Hook, NY, USA, 2019. 5

- [24] Rui Peng, Ronggang Wang, Yawen Lai, Luyang Tang, and Yangang Cai. Excavating the potential capacity of self-supervised monocular depth estimation. In *Proceedings of the IEEE/CVF International Conference on Computer Vision*, pages 15560–15569, 2021. [5](#), [6](#), [7](#)
- [25] Olaf Ronneberger, Philipp Fischer, and Thomas Brox. U-net: Convolutional networks for biomedical image segmentation. In *International Conference on Medical image computing and computer-assisted intervention*, pages 234–241. Springer, 2015. [4](#)
- [26] Aashish Sharma, Loong-Fah Cheong, Lionel Heng, and Robby T Tan. Nighttime stereo depth estimation using joint translation-stereo learning: Light effects and uninformative regions. In *2020 International Conference on 3D Vision (3DV)*, pages 23–31. IEEE, 2020. [2](#)
- [27] Chang Shu, Kun Yu, Zhixiang Duan, and Kuiyuan Yang. Feature-metric loss for self-supervised learning of depth and egomotion. In *European Conference on Computer Vision*, pages 572–588. Springer, 2020. [5](#), [7](#)
- [28] Jaime Spencer, Richard Bowden, and Simon Hadfield. Defeat-net: General monocular depth via simultaneous unsupervised representation learning. In *Proceedings of the IEEE/CVF Conference on Computer Vision and Pattern Recognition*, pages 14402–14413, 2020. [6](#), [7](#)
- [29] Antonio Torralba and Aude Oliva. Depth estimation from image structure. *IEEE Transactions on pattern analysis and machine intelligence*, 24(9):1226–1238, 2002. [3](#)
- [30] Benjamin Ummenhofer, Huizhong Zhou, Jonas Uhrig, Nikolaus Mayer, Eddy Ilg, Alexey Dosovitskiy, and Thomas Brox. Demon: Depth and motion network for learning monocular stereo. In *Proceedings of the IEEE conference on computer vision and pattern recognition*, pages 5038–5047, 2017. [7](#)
- [31] Madhu Vankadari, Sourav Garg, Anima Majumder, Swagat Kumar, and Ardhendu Behera. Unsupervised monocular depth estimation for night-time images using adversarial domain feature adaptation. In *European Conference on Computer Vision*, pages 443–459. Springer, 2020. [1](#), [2](#), [5](#), [6](#)
- [32] Jiaping Wang, Peiran Ren, Minmin Gong, John Snyder, and Baining Guo. All-frequency rendering of dynamic, spatially-varying reflectance. *ACM Trans. Graph.*, 28(5):1–10, 2009. [4](#)
- [33] Kun Wang, Zhenyu Zhang, Zhiqiang Yan, Xiang Li, Baobei Xu, Jun Li, and Jian Yang. Regularizing nighttime weirdness: Efficient self-supervised monocular depth estimation in the dark. In *Proceedings of the IEEE/CVF International Conference on Computer Vision*, pages 16055–16064, 2021. [1](#), [5](#), [6](#), [2](#), [3](#)
- [34] Ruoyu Wang, Zehao Yu, and Shenghua Gao. Planedepth: Self-supervised depth estimation via orthogonal planes. In *Proceedings of the IEEE/CVF Conference on Computer Vision and Pattern Recognition*, pages 21425–21434, 2023. [5](#), [7](#)
- [35] Zian Wang, Jonah Philion, Sanja Fidler, and Jan Kautz. Learning indoor inverse rendering with 3d spatially-varying lighting. In *Proceedings of the IEEE/CVF International Conference on Computer Vision*, pages 12538–12547, 2021. [4](#)
- [36] Jiaxing Yan, Hong Zhao, Penghui Bu, and YuSheng Jin. Channel-wise attention-based network for self-supervised monocular depth estimation. In *2021 International Conference on 3D Vision (3DV)*, pages 464–473. IEEE, 2021. [5](#), [7](#)
- [37] Maoke Yang, Kun Yu, Chi Zhang, Zhiwei Li, and Kuiyuan Yang. Denseaspp for semantic segmentation in street scenes. In *Proceedings of the IEEE conference on computer vision and pattern recognition*, pages 3684–3692, 2018. [2](#)
- [38] Yupeng Zheng, Chengliang Zhong, Pengfei Li, Huan-ang Gao, Yuhang Zheng, Bu Jin, Ling Wang, Hao Zhao, Guyue Zhou, Qichao Zhang, and Dongbin Zhao. Steps: Joint self-supervised nighttime image enhancement and depth estimation. In *2023 IEEE International Conference on Robotics and Automation (ICRA)*, pages 4916–4923, 2023. [1](#)
- [39] Tinghui Zhou, Matthew Brown, Noah Snavely, and David G Lowe. Unsupervised learning of depth and ego-motion from video. In *Proceedings of the IEEE conference on computer vision and pattern recognition*, pages 1851–1858, 2017. [1](#), [2](#), [3](#), [5](#), [6](#), [7](#)

7. Supplementary Material Introduction

This appendix includes additional details and results to support our manuscript. In particular, this appendix is organized as follows:

- In Section 8, we discuss more details about the datasets.
- In Section 9, we show more quantitative results.
- In Section 10, we present additional qualitative results.
- In Section 11, we review failure cases.

8. DataSet Details

Oxford RobotCar-Night and RobotCar-Day: The RobotCar-Night/Day dataset split is from Wang et al. [33]. The RobotCar-Night dataset contains images from the 2014-12-16-18-44-24 folder, which includes 6000 training images and 411 test images. The RobotCar-Day contains images from the 2014-12-09-13-21-02 folder, which includes 2000 training images and 451 test images. All images are cropped to 1152×672 .

nuScenes-Night: From the original nuScenes dataset [1], Wang et al. [33] created the nuScenes-Night dataset split, which contains over 10000 training images and 500 test samples. All images are cropped to 1536×768 .

KITTI: The KITTI [5] is a daytime only dataset. We use the split by Eigen et al. [2], specifically, we uniformly select 10000 images and test LAA-Net on 697 images. All images are in 1242×375 .

Table 7. **Ablation Study:** We test LAA-Net on all images from nuScenes-Night dataset [1] in 40 meters depth range. The best results are in **bold**. The SOTA methods are the same as Table 3.

Method	40 meters – nuScenes-Night			
	absRel	sqRel	RMSE	$\delta_1 < 1.25$
	lower is better			higher is better
Monodepth2	0.116	0.811	3.701	0.876
md4All-AD	0.121	0.881	3.851	0.870
md4All-DD	0.109	0.757	3.606	0.883
LAA-Net	0.098	0.741	3.586	0.906

Table 8. **Ablation Study:** We test LAA-Net on all images from nuScenes-Night dataset [1] in 50 meters depth range. The best results are in **bold**. The SOTA methods are the same as Table 3.

Method	50 meters – nuScenes-Night			
	absRel	sqRel	RMSE	$\delta_1 < 1.25$
	lower is better			higher is better
Monodepth2	0.136	1.361	5.645	0.869
md4All-AD	0.131	1.381	5.728	0.865
md4All-DD	0.122	1.202	5.413	0.876
LAA-Net	0.111	1.198	5.411	0.878

9. Additional Quantitative Results

9.1. Evaluation over Different Distances

Table 7, 8, and 9 are the results of nuScenes-Night dataset [1] with different depth scales. Specifically, we alter the

Table 9. **Ablation Study:** We test LAA-Net on all images from nuScenes-Night dataset [1] in 60 meters depth range. The best results are in **bold**. The SOTA methods are the same as Table 3.

Method	60 meters – nuScenes-Night			
	absRel	sqRel	RMSE	$\delta_1 < 1.25$
	lower is better			higher is better
Monodepth2	0.137	1.364	5.650	0.841
md4All-AD	0.135	1.387	5.731	0.841
md4All-DD	0.122	1.204	5.418	0.855
LAA-Net	0.115	1.201	5.415	0.863

β value mentioned in 3.1 from 80 meters to 40, 50, and 60 meters, respectively. The results show that LAA-Net outperforms SOTA methods in all distances, demonstrating LAA-Net’s robustness under nighttime scenarios.

Table 10, 11 and 12 show the results of RobotCar-Day and RobotCar-Night dataset [19] with depth scales of 40, 50, and 60 meters, respectively. The results affirm that *LAA-Net can accurately estimate the depth under both daytime and nighttime scenarios despite the varying depth scales*. Admittedly, in Table 10, Monodepth2 performs better than LAA-Net in RMSE during the day. However, we significantly outperform Monodepth2 in RMSE during the night. Notably, for all daytime results in Table 11 and Table 12, our model outperforms Monodepth2 in all metrics. This is because Monodepth2 considers occluded pixels, which play a more important role in short-distance conditions than in long-distance conditions. For all nighttime results, LAA-Net maintains the best accuracy, showcasing our model’s robustness.

9.2. Additional Ablation Study

In Table 13, we replace the DispNet encoder of LAA-Net with ResNet-50 [11], further demonstrating our design choice of using red channel.

We also conduct a study of attenuation item $e^{-\mu d_R}$ (Exponential) in Table 14. While the other parts in Equation 2 remain the same, we first change $e^{-\mu d_R}$ to linear function (Equation 6). And then, we change $e^{-\mu d_R}$ to quadratic function (Equation 7). For the experiment settings, we set $a = 0.0095, b = 0.05$ for Equation 6 [12]. We then set $a = 0.0095, b = 0.05, c = 1.0$ for Equation 7 [12]. All other experiment settings stay the same as in Table 2. The results demonstrate our design choice of using $e^{-\mu d_R}$ as attenuation item.

$$I = I_0 \frac{1}{a \times d_R + b} \quad (6)$$

$$I = I_0 \frac{1}{a \times d_R^2 + b \times d_R + c} \quad (7)$$

Table 15 presents the ablation study with different strategies to choose μ in Equation 2; For the first strategy, we set μ to a fixed value. To ensure a fair comparison, we respectively set μ to 0.05, 0.025, and 0.0125, which are selected

Table 10. **Ablation Study:** LAA-Net on all images from the RobotCar-Day/Night dataset [33] and set depth range up to 40 meters. The best results are in **bold**. The models are the same as Table 2. AD and DD mean different training strategies for md4All.

Method	40m – RobotCar - day				40m – RobotCar - night			
	absRel	sqRel	RMSE	$\delta_1 < 1.25$	absRel	sqRel	RMSE	$\delta_1 < 1.25$
	lower-better		higher-better		lower-better		higher-better	
Monodepth2	0.118	0.614	3.034	0.865	0.3022	1.702	4.984	0.461
md4All-AD	0.110	0.650	3.130	0.881	0.1203	0.762	3.531	0.859
md4All-DD	0.112	0.618	3.125	0.872	0.1206	0.723	3.479	0.849
LAA-Net	0.105	0.612	3.102	0.897	0.1191	0.707	3.465	0.887

Table 11. **Ablation Study:** LAA-Net on all images from the RobotCar-Day/Night dataset [33] and set depth range up to 50 meters. The best results are in **bold**. The models are the same as Table 2. AD and DD mean different training strategies for md4All.

Method	50m – RobotCar - day				50m – RobotCar - night			
	absRel	sqRel	RMSE	$\delta_1 < 1.25$	absRel	sqRel	RMSE	$\delta_1 < 1.25$
	lower-better		higher-better		lower-better		higher-better	
Monodepth2	0.119	0.670	3.164	0.863	0.3029	1.724	5.038	0.458
md4All-AD	0.111	0.707	3.248	0.880	0.1223	0.851	3.723	0.857
md4All-DD	0.113	0.648	3.206	0.871	0.1219	0.784	3.604	0.848
LAA-Net	0.106	0.642	3.155	0.886	0.1193	0.779	3.591	0.885

Table 12. **Ablation Study:** LAA-Net on all images from the RobotCar-Day/Night dataset [33] and set depth range up to 60 meters. The best results are in **bold**. The models are the same as Table 2. AD and DD mean different training strategies for md4All.

Method	60m – RobotCar - day				60m – RobotCar - night			
	absRel	sqRel	RMSE	$\delta_1 < 1.25$	absRel	sqRel	RMSE	$\delta_1 < 1.25$
	lower-better		higher-better		lower-better		higher-better	
Monodepth2	0.120	0.698	3.215	0.863	0.3029	1.728	5.045	0.458
md4All-AD	0.112	0.731	3.291	0.880	0.1231	0.903	3.812	0.857
md4All-DD	0.113	0.661	3.234	0.871	0.1225	0.824	3.664	0.848
LAA-Net	0.108	0.647	3.210	0.882	0.1204	0.809	3.659	0.881

Table 13. **Ablation Study of Using Red Channel:** Using red channel images from the RobotCar-Night dataset [33] and the depth range is up to 80m. ResNet-50 means the encoder in the baseline model is replaced by ResNet-50. R means Red Channel, so do B (Blue Channel) and G (Green Channel), RGB (normal image with all three channels). The best results are in **bold**.

Methods	Abs Rel	Sq Rel	RMSE	RMSE log
	lower is better			
ResNet-50	0.137	0.815	3.821	0.191
ResNet-50+RGB	0.125	0.803	3.665	0.186
ResNet-50+B	0.122	0.795	3.651	0.180
ResNet-50+G	0.121	0.791	3.650	0.177
ResNet-50+R	0.120	0.788	3.641	0.171

Table 14. **Ablation Study of Attenuation Item:** Using red channel images from the RobotCar-Night dataset [33] and the depth range is up to 80m. Linear means that we treat light attenuation as a linear function. And so do Quadratic and Exponential. The best results are in **bold**.

Methods	Abs Rel	Sq Rel	RMSE	RMSE log
	lower is better			
LAA-Net+Linear	0.122	0.855	3.741	0.187
LAA-Net+Quadratic	0.129	0.857	3.735	0.183
LAA-Net+Exponential	0.117	0.786	3.633	0.160

based on 80 meters’ depth range. For the second strategy, we set μ as a learnable parameter, which is the implementation of LAA-Net.

According to Table 15 and 16, setting μ and λ as learnable parameters gives the best accuracy. This is because

Table 15. **Ablation Study of μ :** Using different μ on RobotCar-Night dataset [33] and the depth range is up to 80m. The best results are in **bold**.

Methods	Abs Rel	Sq Rel	RMSE	RMSE log
	lower is better			
$\mu=0.1$	0.139	0.905	4.875	0.201
$\mu=0.05$	0.125	0.889	4.362	0.185
$\mu=0.025$	0.120	0.867	4.257	0.181
Learnable μ	0.117	0.786	3.633	0.160

Table 16. **Ablation Study of λ :** Using different λ on RobotCar-Night dataset [33] and the depth range is up to 80m. The best results are in **bold**.

Methods	Abs Rel	Sq Rel	RMSE	RMSE log
	lower is better			
$\lambda = 0.01$	0.358	0.935	9.182	0.980
$\lambda = 0.1$	0.227	0.895	4.775	0.677
$\lambda = 0.003$	0.195	0.881	3.951	0.451
Learnable λ	0.117	0.786	3.633	0.160

each pixel of the same input image may represent a unique light attenuation condition; dynamically assigning distinct μ and λ values to each pixel enables each pixel to automatically adjust to its own light attenuation conditions. To determine the optimal value for the parameter g in Equation 4, we conducted empirical tests using various values. Our results, presented in Table 17, indicate that setting g to 1.3938 yields the highest accuracy.

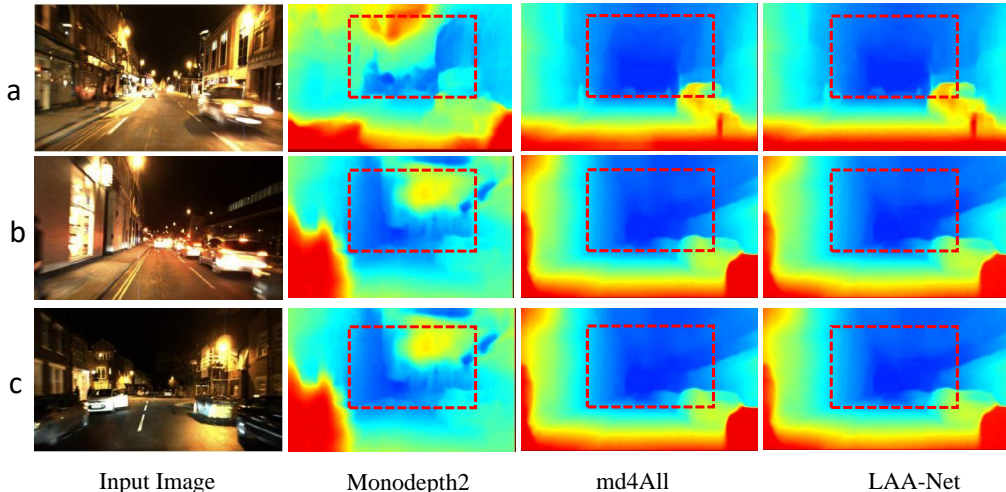


Figure 5. **Qualitative Results - RobotCar-Night:** Depth estimated on three different test images (column: Input Image) using our approach (column: LAA-Net) in comparison with two other methods (remaining columns).

Table 17. **Ablation Study of g :** Using different g on RobotCar-Night dataset [33] and the depth range is up to 80m. The best results are in **bold**.

Methods	Abs Rel	Sq Rel	RMSE	RMSE log
	lower is better			
$g = 0.5$	0.921	0.895	6.175	0.710
$g = 0.1$	0.550	0.891	5.587	0.515
$g = 0.01$	0.515	0.887	5.251	0.355
$g = 1.5$	0.873	0.901	5.891	0.689
$g = 1.3938$	0.117	0.786	3.633	0.160

Table 18. **Ablation Study of using different Channel on RobotCar-Dusk dataset [33]:** R means Red Channel, so do B (Blue Channel) and G (Green Channel), RGB (regular image with all three channels). The best results are in **bold**.

Methods	Abs Rel	Sq Rel	RMSE	RMSE log
	lower is better			
LAA-Net+RGB	0.157	0.978	4.857	0.212
LAA-Net+B+R	0.148	0.851	4.437	0.190
LAA-Net+G+R	0.144	0.801	4.337	0.183
LAA-Net+B+G	0.141	0.793	4.241	0.185
LAA-Net+B	0.109	0.648	4.237	0.179
LAA-Net+G	0.105	0.635	4.232	0.168
LAA-Net+R	0.090	0.605	3.991	0.151

9.3. Low Light Condition in Daytime

We conducted an ablation study with the RobotCar-Dusk dataset, which includes images taken at 16:34 on 02/20/2015. *Although captured during the daytime, these images reflect low-light conditions.*

From the results in Table 18, we can observe a consistent trend with Table 6: LAA-Net+R achieves the best performance compared to all other single channels and channel combinations.

10. Additional Qualitative Results

Figure 5 shows the results on the RobotCar-Night dataset, demonstrating that our model provides more accurate nighttime MDE results compared to others. For instance, The red boxes in Figure 5 - a,b,c demonstrate our model’s ability to accurately handle varying lighting conditions.

In Figures 6, we use nuScence-Night dataset to compare LAA-Net with SOTA methods: Monodepth2 [8] and md4All [4]. From the results, LAA-Net shows sharper details for the roads and cars, showcasing LAA-Net’s ability to accurately handle varying light conditions under nighttime scenarios.

Notably, the input images are particularly challenging as they were taken in extremely dark environments. However, LAA-Net can still provide robust results under those extreme night conditions.

11. Failure Cases

LAA-Net performs well under nighttime scenarios, but there’s room for improvement with specific corner cases. For example, Figure 7 shows two instances of the failure cases. In the input images, halos originating from road lamps and other car headlights are the main reasons for these failure cases. These halos give rise to shadows and reflections, which could affect the light attenuation item (Equation 2) in RCA loss, leading to compromised depth estimation results.

The halo issue is commonly known as one of the most challenging conditions in nighttime depth estimation [33]. From Figure 7, we can see that SOTA method md4All [4] produces similar depth results as LAA-Net, demonstrating that SOTA methods may not be able to handle the failure case well.

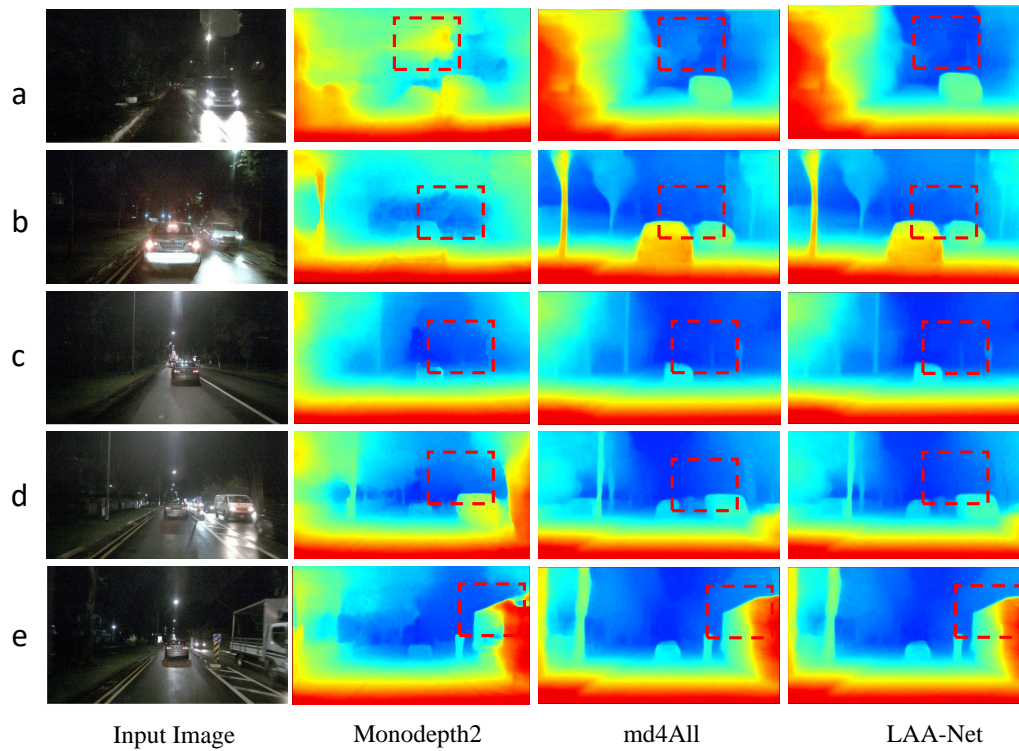


Figure 6. **Qualitative Results - nuScence-Night:** Depth estimated on five different test images (column: Input) using our approach (column: LAA-Net) in comparison with two SOTA methods (remaining columns).

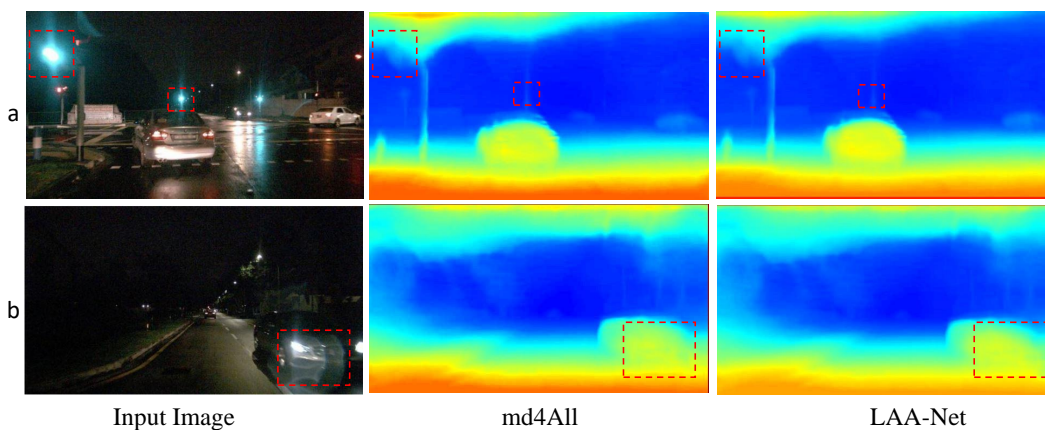


Figure 7. **Failure Cases - nuScence-Night:** Comparison between LAA-Net and md4All[4]. Red boxes show the halos because of road lamps and car headlights in the input image, which may cause failure for both LAA-Net and md4All.